Pergamon

Int. J. Heat Mass Transfer. Vol. 40, No. 8, pp. 1795–1805, 1997

0017–9310/97 $17.00 + 0.00

PII: S0017–9310(96)00251–7

Optimal geometric arrangement of staggered plates in forced convection

A. J. FOWLER

Mechanical Engineering Department, University of Massachusetts Dartmouth, North Dartmouth, MA 02747-2300, U.S.A.

and

G. A. LEDEZMA and A. BEJAN†

Department of Mechanical Engineering and Materials Science, Duke University, Durham, NC 27708-0300, U.S.A.

(*Received* 15 *March* 1996 *and in final form* 9 *July* 1996)

Abstract—This paper reports the results of an experimental and numerical study of the optimal geometric arrangement of staggered parallel plates in a fixed volume with forced convection heat transfer. The objective of the geometric optimization effort is to maximize the total heat transfer rate between the given volume and the given external flow, when the maximum temperature at a point inside the volume cannot exceed a certain level. The geometric arrangement was varied systematically, by changing the spacing between plates, the number of plates installed in one row, the plate swept length, and the degree to which the plates are staggered. In the first part of the study, it is demonstrated experimentally that there exists an optimal spacing between two adjacent row of plates. Experimental results are reported for air in the range $1000 \leqslant Re_L \leqslant 6000$, where L is the swept length of the fixed volume. In the second part of the study, extensive numerical results support and extend these findings to $100 \leqslant Re_L \leqslant 10\,000$. In addition, it is shown that there is an optimal way to stagger the plates. In the concluding part of the paper, the optimal spacing and maximum heat transfer rate results are correlated based on the theoretical method of intersecting the two asymptotes (small spacing, large spacing) of the geometric arrangement.

1. INTRODUCTION

The development of cooling techniques for electronic equipment places a new emphasis on 'augmentation' as a fundamental problem in the field of heat transfer [1]. The new aspect is that in electronic packaging the augmentation of heat transfer must be accomplished subject to volume constraint. The objective is to assemble as much circuitry as possible (i.e. maximum heat generation rate) in a given space exposed to a given coolant, such that the maximum temperature attained by a certain point in that space (the hot spot) does not exceed an allowable level. This type of heat transfer augmentation is 'global', i.e. not local or elemental as in the classical techniques (e.g. fins, ribbed surfaces).

It is important to note that the volume-constrained augmentation of heat transfer offers a new optimization opportunity: in some applications it may be possible to vary the relative positions of the electronic components in the fixed space such that the total heat generation rate can be increased. For example, if the interstitial spaces permit, more components can be placed in those regions where the temperatures are lower than the hot-spot temperature.

This opportunity was recognized in several fundamental studies of cooling techniques. The simplest class of fundamental results in this new area is represented by the optimal spacing between two adjacent components when a large number of such components are mounted in a fixed space. For natural convection cooling the optimal spacing between vertical smooth plates was developed by Bar Cohen and Rohsenow [2], Bejan [3], Kim *et al.* [4] and Anand *et al.* [5]. The optimal spacing between horizontal cylinders in natural convection was determined numerically and experimentally by Bejan *et al.* [6]. For forced convection cooling, the literature contains results for the optimal spacing between parallel plates with smooth surfaces [7–10], plates with flush-mounted or protruding heat sources [11] and cylinders or pin fins mounted in a fixed space [12, 13].

The optimal spacings for components in a fixed volume are also relevant to the geometric optimization of heat exchangers. For example, the fin-to-fin spacings of the air cooled heat sink for an electronic module is relevant to selecting the tube-to-tube spacing for the core of a heat exchanger. It is both appro-

† Author to whom correspondence should be addressed.

NOMENCLATURE

A	dimensionless contact area, equation (1)
b	plate swept length [m], Fig. 1
B	plate length (bundle width) [m]
D	spacing between L-long parallel plates [m]
H	bundle height [m], Fig. 1
k	fluid thermal conductivity [W (m K)$^{-1}$]
L	bundle flow length [m], Fig. 1
L_d	downstream length [m]
L_u	upstream length [m]
N	number of plate surfaces facing the elemental channel, Fig. 1
P	pressure [N m^{-2}]
q	heat transfer rate per elemental channel [W]
$\tilde{q}$	dimensionless overall thermal conductance, equation (3)
Q	total heat transfer rate from the bundle [W]
Re_L	Reynolds number, equation (2)
t	plate thickness [m], Fig. 1
T	temperature [K]
T_w	plate temperature [K]
$\bar{T}$	average surface temperature [K]
T_∞	free stream temperature [K]
u, v	velocity components [m s^{-1}]
U	uncertainty
U_∞	free stream velocity [m s^{-1}]
W	channel spacing [m], Fig. 1
$\tilde{W}$	dimensionless channel spacing, equation (1)
x, y	cartesian coordinates [m].

Greek symbols

β	stagger parameter [m], Fig. 1
β_{max}	maximum stagger parameter [m], equation (10)
ΔP	pressure difference scale $(1/2)(\rho U_\infty^2)$, [N m^{-2}]
θ	dimensionless temperature, equation (9)
ν	kinematic viscosity [m^2 s^{-1}]
$()_{max}$	maximum
$()_{opt}$	optimal
$(\tilde{})$	dimensionless variables, equations (8)–(10).

priate and timely that we extend the volume-constrained optimization method to one of the most common types of heat exchanger surfaces, namely, the staggered plates parallel to the incident flow, or the staggered flattened tubes. The literature on the heat transfer and pressure drop characteristics of this surface type is sizable, and can be reviewed in refs. [14–16]. More recent studies such as those of Guglielmini *et al.* [17] and Tanda [18], have focused on the interaction of the boundary layers of staggered plates. This interaction is the key to the optimization of any geometric arrangement.

The present study focuses on the geometric optimization of staggered plates in a fixed volume. The problem is treated in a most fundamental (geometric) sense, without specific reference to an application (electronics cooling, compact heat exchangers). The paper has three parts. In the first, we demonstrate experimentally that optimal arrangements exist. For example, we show that the optimal spacing between adjacent rows of plates can be optimized. In the second part, the heat and fluid flow performance of the assembly is simulated numerically. The effect of varying the geometry is investigated by changing one geometric parameter at a time, and comparing many geometric configurations that differ only slightly from one another. The objective of the numerical part was to generate a large volume of optimization results that reveal the correct trends (scaling laws). In the concluding part of the study, we show that the optimal spacings can be correlated based on the same theory that produced scaling-correct correlations for optimal spacings in simpler forced convection configurations.

2. GEOMETRIC AND OPERATIONAL PARAMETERS

The geometric parameters of the space filled with staggered parallel plates are defined in Fig. 1. The total volume occupied by this ensemble is fixed: it has the length L in the flow direction, the 'height' H in the direction perpendicular to the flow and the plates, and the width B in the direction perpendicular to the plane of Fig. 1. The plates are identical: each has the swept length b, thickness t and breadth B. The fluid and its free stream velocity U_∞ are specified.

The geometric arrangement of the plates has four degrees of freedom: the spacing W between two adjacent rows, the number of plates mounted in one row of length L, the plate dimension b, and the stagger parameter β (Fig. 1). It is convenient to express two of these degrees of freedom in dimensionless form by defining

$$\tilde{W} = \frac{W}{L} \quad A = \frac{Nb}{L} \tag{1}$$

where $\tilde{W}$ is the dimensionless spacing, and A is the dimensionless heat transfer area that faces the elemental channel indicated by the dashed lines in Fig. 1. In the A definition, N is the number of plates that are wetted by the flow through a single elemental channel

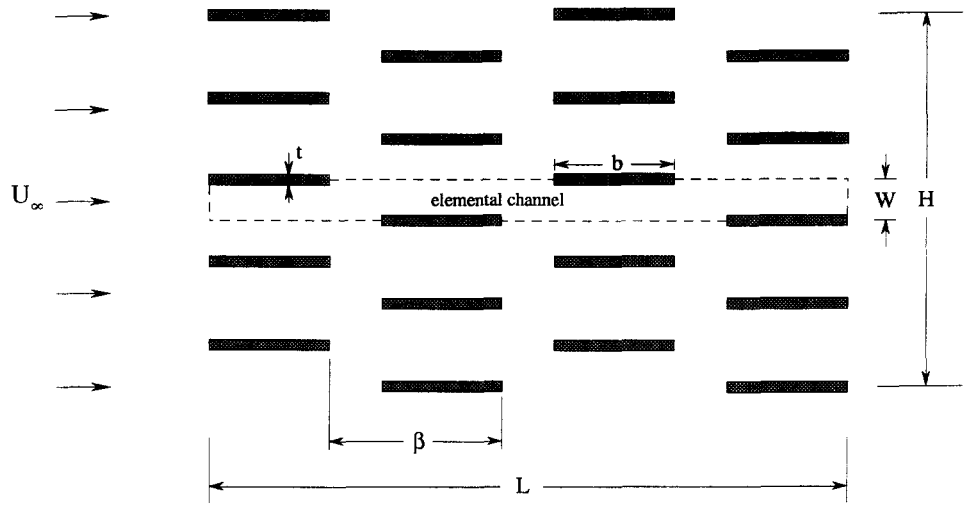

Fig. 1. The geometric parameters of a volume filled with staggered parallel plates subjected to forced convection in a parallel free stream.

(e.g. $N = 4$ in Fig. 1). Clearly, $A = 2$ represents the limit where the plate ends (edges) touch. The free-stream velocity can vary, and is represented by the Reynolds number based on the flow length of the given volume,

$$Re_L = \frac{U_\infty L}{\nu}. \tag{2}$$

The geometry of the assembly mounted in the volume $L \times H \times B$ can be changed by varying $\tilde{W}$, A, N or β, or a combination of these parameters. We are interested in the geometric arrangement that maximizes the overall thermal conductance between the ensemble (plates, with the highest temperature equal to T_w) and the approaching fluid (T_∞). The thermal conductance is $Q/(T_w - T_\infty)$, where Q is the total heat transfer rate, $Q = qH/W$ and q is the heat transfer rate from the elemental channel (Fig. 1). Since the overall dimensions of the volume are fixed, to maximize the overall thermal conductance means to maximize the ratio $q/[W(T_w - T_\infty)]$ of the elemental channel. A dimensionless alternative to this ratio, which we found suitable in the experimental and numerical investigations described next, is

$$\tilde{q} = \frac{q}{W(T_w - T_\infty)kB/L}. \tag{3}$$

Another way to arrive at this objective function is to think of $L \times H \times B$ as a given volume that is to be filled with heat generating components while the temperature T_w is fixed. To maximize the overall heat transfer rate is the same as maximizing the average heat generation rate per unit volume, $Q/(LHB) = q/(WBL)$, which is represented by the dimensionless $\tilde{q}$ defined in equation (3) because L is fixed.

3. EXPERIMENTAL RESULTS

The objective of the experimental phase of our study was to demonstrate through direct measurements that the geometric arrangement of the parallel plates can be optimized for maximum $\tilde{q}$. In other words, our first objective was to prove the *existence* of an optimal geometric arrangement. To generate a large volume of design information on the optimal arrangement as a function of the variable parameters of the ensemble was the objective of the numerical phase of this investigation (Section 4).

The main features of the experimental apparatus are illustrated in Fig. 2. The apparatus is a suction-type wind tunnel fitted in its test section with a bundle of heated plates. The volume occupied by the bundle was the same in all the experiments; however, the total number and the geometric arrangement of the plates inside the bundle varied from one experiment to the next. We tested bundles with 4, 6, 8, 10 and 14 plates; however, in all the bundles the elemental channel had $N = 4$. The size of the largest bundle (number of plates = 14) and the plates in the elemental channel ($N = 4$) were constrained by the construction of the test section of the tunnel. The stagger parameter was maximum (β_{max}) in all the experiments. In summary, the geometries tested experimentally had only one degree of freedom: the row spacing $\tilde{W}$.

The lower part of Fig. 2 shows the test bundle with six plates and $A = 1$. Each plate was a thin thermofoil heater MINCO HR5334 R17.2L12A (resistance 17.2 Ω), which was sandwiched between two aluminum strips. The heater and the strips were bound using a highly conductive cement (#6 RTV). The plates were heated identically: they were connected in parallel and powered by a variable autotransformer that produced voltages between 0 and 140 V.

The experiments were conducted at four air speeds corresponding to the Reynolds numbers $Re_L = 1000$,

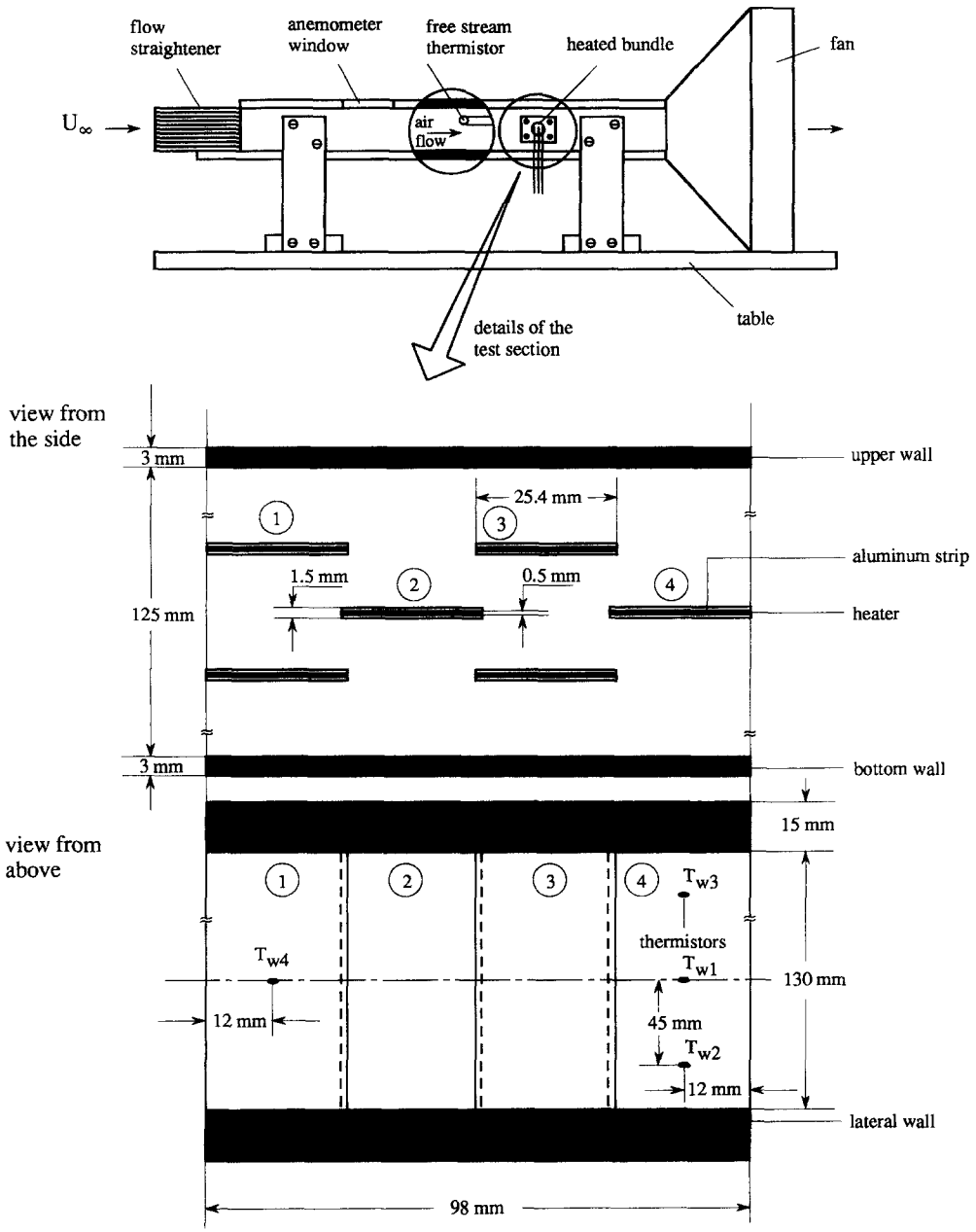

Fig. 2. The principal features of the experimental apparatus and its test section.

2000, 4000 and 6000, which indicate laminar boundary layer flow over the swept length L. The air stream was generated by the wind tunnel, which was built in our laboratory. The internal dimensions of the wind tunnel are $125 \times 130 \times 600$ mm. The air speed was measured using a Taylor anemometer with an uncertainty of 5%.

The temperature was measured with five precision thermistors YSI 44004 (resistance 2250 Ω at 25°C), which were calibrated between 20 and 80°C in our laboratory. The bias limit of our temperature measurements was ± 0.001K. It was deduced from the resistance vs temperature response measured during the calibration of each thermistor [$dT/dR = (-1/14)$K Ω^{-1}] and from the 0.01 Ω resolution of the HP3468B ohmmeter with which we read the thermistor resistance.

The bottom of Fig. 2 shows the thermistor positions. Three thermistors were attached to the upper surface of one of the trailing plates in the bundle, along the midline of the surface. Their readings are labeled T_{w1}, T_{w2}, and T_{w3}. A fourth thermistor (T_{w4}) was placed in the middle of the upper surface of one of the upstream plates. The fifth thermistor was positioned 65 mm upstream of the bundle, to monitor the temperature of the approaching free stream (T_∞). In the case of the thermistors embedded in the aluminum plate surface, the contact gap between thermistor

and aluminum was filled with highly conductive heat sink compound. The outer side of the thermistor was covered flush with a small strip of aluminum foil, which was glued (with heat resistant plastic cement) to the aluminum surface.

Each run began with setting the voltages for the plate heaters and the fan. We monitored for two hours the changes in the temperature readings ($T_{w1}, T_{w2}, T_{w3}, T_{w4}, T_\infty$) and the power input to the plate heaters. We assumed that the steady state was reached, and the actual measurements could start, when the changes in the temperature readings were less than 0.2°C. In each experimental run we took 25 resistance readings from each thermistor, and 25 voltage readings from the plate heaters—all during a period of 30 min. The temperature range of our experiments is bordered from below by 25°C, which was one of the air stream temperature readings, and from above by 70°C, which was reached by one of the trailing plates.

In equation (3) we used T_{w1} in place of T_w to calculate the overall thermal conductance $\tilde{q}$. The position of the T_{w1} thermistor is shown in Fig. 2: this choice was not critical because the temperature of the trailing plate was essentially uniform. In all the runs, the maximum difference between T_{w1}, T_{w2} and T_{w3} was less than 3°C. The maximum nonuniformity of 3°C occurred when $T_{w1} = 70°C$ and $T_{w1} - T_\infty = 45°C$. In other words, the maximum relative nonuniformity in $(T_{w1} - T_\infty)$ was 7%. The temperature of the plates in the central rows (Fig. 2) were not measured because they fall between T_{w4} and T_{w1}; in other words, the relative nonuniformity of temperature over the central plates is expectedly less than 7%. The air properties were evaluated at the film temperature $(\bar{T}_w + T_\infty)/2$, where $\bar{T}_w = (T_{w1} + T_{w2} + T_{w3} + T_{w4})/4$.

We evaluated the experimental uncertainties using the procedure described by Moffat [19] and the propagation line of Kline and McClintock [20]. The bias limit of 0.001K determined during the calibration of the thermistors agrees with the bias limit reported by Howle *et al.* [21] and an instrumentation handbook [22]. The bias limits for the voltage across the plate heaters and their resistance are 0.001 V and 0.1 Ω. The length measurements (L, H, B) have a bias limit of 1 mm. The uncertainty in the tabulated properties of air (k, ν) was taken as 5%.

The precision limit of measured quantities such as the temperature and the voltage power dissipated by the heaters was estimated as two times the standard deviation. In the case of temperature the precision limit values were as high as 0.4K, which made the bias limit contribution negligible. The estimated uncertainty in Reynolds number was 7% in all the runs. The calculated uncertainty in the overall thermal conductance was always less than 7.6%.

Figure 3 illustrates our experimental results for the overall thermal conductance, as a function of spacing ($\tilde{W}$) and air speed (Re_L). Since in the experiments there is flow around the bundle, in the calculation of

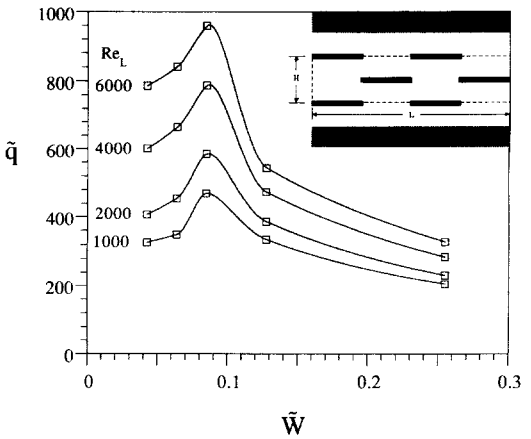

Fig. 3. Experimental results showing the effect of plate-to-plate channel spacing and Re_L on the overall thermal conductance ($A = 1, N = 4, \tilde{\beta} = 1, Pr = 0.72$).

$\tilde{q}$ (cf. equation (3)) we used only the heat released through the surfaces present in the volume $L \times H \times B$ shown in the inset of Fig. 3. We chose this volume in order to make the geometry of the tested bundle approach as much as possible the geometry sketched in Fig. 1.

The results of Fig. 3 are for the test bundle with $N = 4$, $A = 1$, and $\beta = \beta_{max}$. It is clear that when the air speed and all the other parameters (except $\tilde{W}$) are fixed, there is an optimal channel spacing $\tilde{W}$ such that the overall thermal conductance is maximized. In Section 5 we show that these results agree qualitatively and quantitatively with the corresponding results based on the numerical study that is described next.

4. NUMERICAL RESULTS

We simulated numerically the heat and fluid flow fields for the system of Fig. 1 in the laminar range represented by $10^2 \leqslant Re_L \leqslant 10^4$. In view of the plate dimension b assumed in the simulations, this Re_L range corresponds to $1.6 \leqslant U_\infty b/\nu \leqslant 5000$. At such low Reynolds numbers the wake behind each plate is straight (e.g. ref. [23]), and there is no mass flow across the long boundaries of the elemental channel sketched in Fig. 1. We further assumed that there are enough elemental channels in the bundle ($H \gg W$) such that the flow through a single channel is representative of (or a repeating building block in) the flow through the complete bundle. Consequently, we conducted our numerical work in the two-dimensional computational domain represented by one elemental channel ($L \times W$) fitted with an upstream section ($L_u \times W$) and downstream section ($L_d \times W$). The lengths L_u and L_d were selected based on an accuracy test described later in this section.

The equations for the conservation of mass, momentum and energy in the two-dimensional steady flow of a fluid with nearly constant properties are

$$\frac{\partial u}{\partial x}+\frac{\partial v}{\partial y}=0 \tag{4}$$

$$u\frac{\partial u}{\partial x}+v\frac{\partial u}{\partial y}=-\frac{1}{\rho}\frac{\partial P}{\partial x}+\nu\nabla^2 u \tag{5}$$

$$u\frac{\partial v}{\partial x}+v\frac{\partial v}{\partial y}=-\frac{1}{\rho}\frac{\partial P}{\partial y}+\nu\nabla^2 v \tag{6}$$

$$u\frac{\partial T}{\partial x}+v\frac{\partial T}{\partial y}=\alpha\nabla^2 T \tag{7}$$

where $\nabla^2=\partial^2/\partial x^2+\partial^2/\partial y^2$, and x is aligned with the flow direction (U_∞ in Fig. 1). In order to select the appropriate nondimensionalization of the phenomenon *near* the optimal geometric configuration we relied on the numerical approach developed in earlier studies [8, 24]: specifically, (i) the conclusion that near the optimum the elemental channel looks 'long' such that the boundary layers meet in the middle of the channel (i.e. viscous diffusion has time to travel W entirely); and (ii) the pressure difference across the bundle (L) is $\Delta P=(1/2)\rho U_\infty^2$. This pressure difference is particularly accurate in the case of wide bundles ($H\gg W$, as assumed above). The constant pressure difference captures the physics of the geometric optimum: larger W values allow larger flow rates through the elemental channel; however, since the channel volume increases the heat transfer rate per unit of channel volume decreases. In the opposite extreme, when W approaches zero, the channel flow rate vanishes and so does the channel heat transfer rate. This is why there is an intermediate (optimal) channel spacing for maximum heat transfer per unit volume. In conclusion, we used the nondimensional variables

$$(\tilde{x},\tilde{y})=\frac{(x,y)}{L}\quad(\tilde{u},\tilde{v})=\frac{(u,v)}{(\Delta P/\rho)^{1/2}} \tag{8}$$

$$\tilde{P}=\frac{P}{\Delta P}\quad\theta=\frac{T-T_\infty}{T_w-T_\infty}. \tag{9}$$

The flow boundary conditions were: $\tilde{P}=1$ at the inlet of the computational domain ($\tilde{x}=0$); zero normal stress at the outlet [$\tilde{x}=(L_u+L+L_d)/L$]; free slip (zero shear) and zero flow penetration along the imaginary planes between the elemental channel and the adjacent channels; no slip and no flow penetration on all the plate surfaces; and free slip and no penetration on the longitudinal boundaries of the upstream and downstream sections of the computational domain. The temperature boundary conditions were $\theta=1$ on the plate surfaces, and $\theta=0$ at the inlet ($\tilde{x}=0$). The remaining portions of the boundary were modeled as adiabatic.

Our numerical method was developed and documented during the course of similar numerical optimization studies [8, 24], and consisted of two steps. In the first, we developed and tested our own finite-difference code, the results of which we used as benchmark. In the second, we used an existing finite element package [25] to generate the large volume of numerical results (i.e. simulations for many geometries, one differing only slightly from the next), which were needed during the optimization phase of our numerical work. The finite-element results were tested against the benchmark results developed in the initial step.

The numerical optimization results reported later in this section were developed based on the finite element package. The grid was uniform in the $\tilde{x}$ direction and nonuniform in the $\tilde{y}$ direction. It was double-graded so as to put more nodes near the plate surfaces, to capture the boundary layers. Grid refinement tests at $Re_L=10^2$ and 10^3 indicated that the solution was insensitive to further grid doubling in $\tilde{x}$ or $\tilde{y}$ (with changes in the channel heat transfer rate of less than 1%) when we used 100 nodes per unit length (L) in the $\tilde{x}$ direction, and an average of 100 nodes per unit length in the $\tilde{y}$ direction (averaged over the nonuniformity of the grid). At $Re_L=10^4$ the solution was insensitive to further grid doubling if we used 200 nodes per unit length in both directions; in this case, however, the solution converged significantly faster at 300 nodes per unit length in both $\tilde{x}$ and $\tilde{y}$, which was the grid that we selected. Another set of accuracy tests indicated that the channel heat transfer rate was relatively insensitive (with changes less than 1%) to further doubling of the upstream and downstream lengths of the computational domain when $L_u/L=0.1$ and $L_d/L=0.3$. Finally, since the flow and energy equations are weakly coupled, we solved the flow problem first and the heat transfer problem second. Complete runs varied from 2 to 10 min of CPU time on a DEC alpha station.

We developed complete numerical solutions for the flow and heat transfer problems for $Pr=0.72$ and $Re_L=10^2, 10^3$ and 10^4. Our objective was to document systematically the effect on $\tilde{q}$ of each of the four geometric degrees of freedom, $\tilde{W}$, A, N and $\tilde{\beta}$, where

$$\tilde{\beta}=\frac{\beta}{\beta_{max}}\quad\text{and}\quad\beta_{max}=\frac{L-b}{N-1}. \tag{10}$$

The relative stagger parameter varies from $\tilde{\beta}=0$ (plates in line) to $\tilde{\beta}=1$ (perfectly staggered plates, e.g. Fig. 2). During each sequence of runs we varied only one geometric parameter while holding the other geometric and flow parameters fixed.

The strongest effect on the overall thermal conductance is due to varying the channel spacing $\tilde{W}$. This effect is illustrated in Fig. 4 for $A=0.7$, $N=4$, $\tilde{\beta}=1$ and $Re_L=10^3$. The effect is qualified as 'strong' because if the optimal spacing is missed by a factor of 2 or 1/2, the resulting thermal conductance is only about half of what it could be.

We repeated the optimization series of Fig. 4 for 14 additional combinations of A and Re_L, which cover the range $0.5\leqslant A\leqslant 1.3$ and $10^2\leqslant Re_L\leqslant 10^4$. In each series we located the optimal spacing by fitting the three highest $\tilde{q}$ points with a parabola and solving $\partial\tilde{q}/\partial\tilde{W}=0$. The resulting $\tilde{W}_{opt}$ values are summarized in Fig. 5. The optimal spacing decreases as Re_L

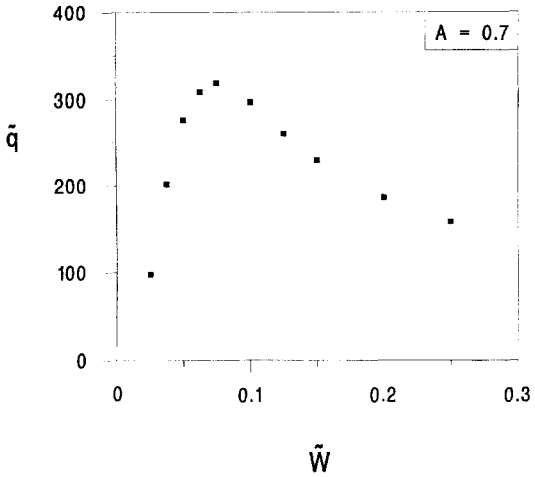

Fig. 4. Numerical results for the effect of channel spacing on the overall thermal conductance ($A = 0.7$, $N = 4$, $\tilde{\beta} = 1$, $Re_L = 10^3$, $Pr = 0.72$).

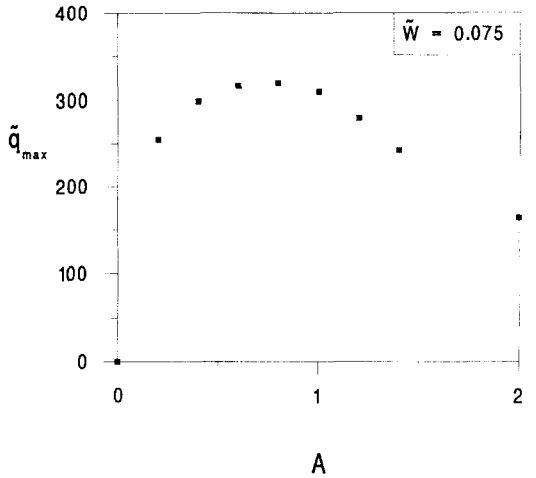

Fig. 6. The effect of channel heat transfer area (A) on the overall thermal conductance ($\tilde{W} = 0.075$, $N = 4$, $\tilde{\beta} = 1$, $Re_L = 10^3$, $Pr = 0.72$).

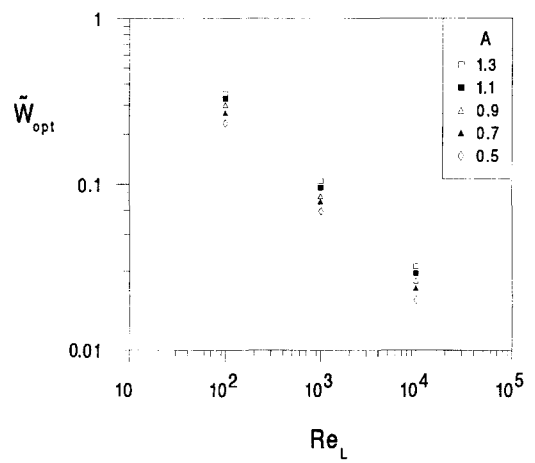

Fig. 5. The effect of coolant flow rate (Re_L) and channel heat transfer area (A) on the optimal spacing for maximum overall thermal conductance ($N = 4$, $\tilde{\beta} = 1$, $Pr = 0.72$).

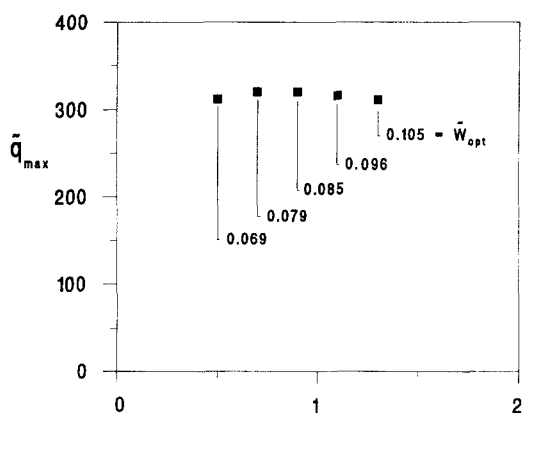

Fig. 7. The effect of the channel heat transfer area A on the maximum overall thermal conductance at optimal spacing ($N = 4$, $\tilde{\beta} = 1$, $Re_L = 10^3$, $Pr = 0.72$).

increases: in fact, as we shall see in equation (12), $\tilde{W}_{opt}$ is closely proportional to $Re_L^{-1/2}$. The A effect is such that $\tilde{W}_{opt}$ increases only slightly as A increases; however, the apparent weakness of this effect may be due to the narrowness of the A domain.

We studied the A effect in greater detail in the optimization series reported in Fig. 6. This time we fixed the spacing ($\tilde{W} = 0.075$, along with $N = 4$, $\tilde{\beta} = 1$, $Re_L = 10^3$ and $Pr = 0.72$) and varied the area parameter A. Our numerical runs are more numerous near $A \cong 1$ to emphasize the existence of an optimal A at constant $\tilde{W}$. Very important are also the two limits, $\tilde{q} = 163.9$ at $A = 2$, and $\tilde{q} = 0$ at $A = 0$. In the latter, the elemental channel $L \times W$ becomes a channel with continuous solid walls (e.g. ref. [7]). The asymmetry of the $\tilde{q}$ maximum in Fig. 6 is worth noting.

Figure 7 is a different way of looking at the importance of maximizing $\tilde{q}$ with respect to $\tilde{W}$. Each point in this figure ($\tilde{W}_{opt}, A$) was obtained by executing the series illustrated in Fig. 4, by changing A from one series to the next and by determining in each series the $\tilde{W}_{opt}$ that maximizes $\tilde{q}$. An important feature of Fig. 7 is the weak $\tilde{q}$ maximum in the range $0.5 \leqslant A_{opt} \leqslant 1.3$, which corresponds to the optimal spacing range $0.069 \leqslant \tilde{W}_{opt} \leqslant 0.105$. The practical message of Fig. 7 (in combination with Figs. 4 and 6) is that as soon as A is given a value comparable with 1, the critical choice in the maximization of $\tilde{q}$ is the value of $\tilde{W}$. The particular choice of A is unimportant provided W is set at or near W_{opt}.

Note further that since $\tilde{q}_{max}$ is nearly independent of A in Fig. 7, nearly the same maximum $\tilde{q}$ values emerge when $\tilde{q}(\tilde{W}, A)$ is maximized with respect to A while holding $\tilde{W}$ fixed, as was illustrated in Fig. 6. On the other hand, if in Fig. 7 we maximize $\tilde{q}_{max}$ one more time (this time with respect to A), then the twice-maximized overall thermal conductance is $\tilde{q}_{max,max} = 320$, which occurs at $\tilde{W}_{opt} = 0.08$ and $A_{opt} = 0.8$.

The effect of increasing the number of plates in

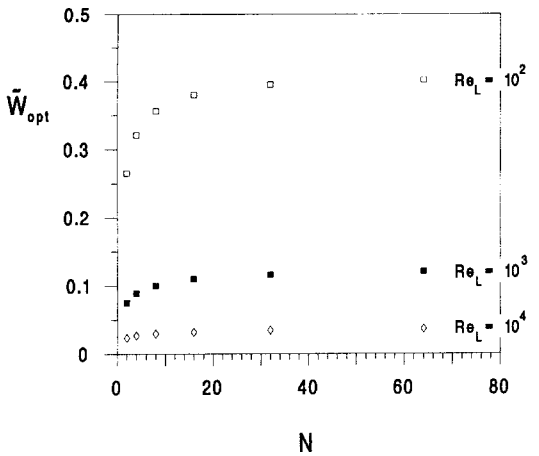

Fig. 8. The effect of the number of plates (N) on the optimal spacing ($A = 1, \tilde{\beta} = 1, Pr = 0.72$).

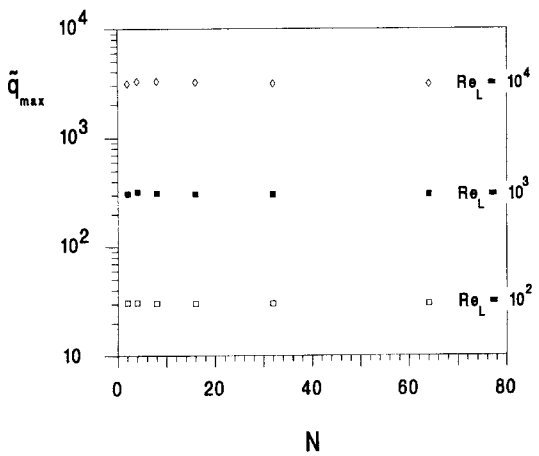

Fig. 9. The maximum thermal conductance corresponding to the optimal spacing shown in Fig. 8, and the effect of changing the number of plates ($A = 1, \tilde{\beta} = 1, Pr = 0.72$).

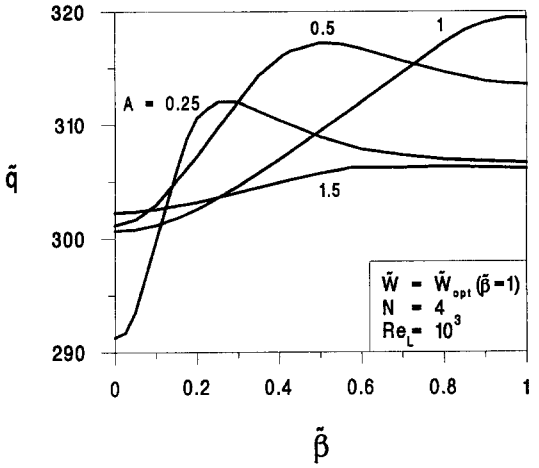

Fig. 10. The effect of the stagger parameter when the spacing is fixed at $\tilde{W}_{opt}$ ($\tilde{\beta} = 1$) ($N = 4, Re_L = 10^3$).

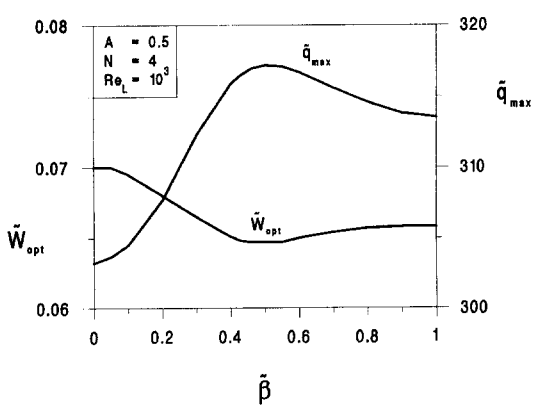

Fig. 11. The effect of the stagger parameter on the optimal spacing and the maximum overall thermal conductance ($A = 0.5, N = 4, Re_L = 10^3$).

each channel (N) is illustrated in Fig. 8. Physically, to increase N while holding A fixed is to divide a fixed plate area into more plates with smaller b values. When N is of the order of 10 or smaller, the optimal spacing increases sensibly as N increases. At sufficiently larger values of N, the optimal spacing is insensitive to further increases in the number of plates. It is interesting that the Re_L effect on $\tilde{W}_{opt}$ continues to be as in Fig. 5, namely $\tilde{W}_{opt} Re_L^{1/2} =$ constant, regardless of whether N is large or small.

The maximized overall conductances that correspond to the optimal spacings of Fig. 8 are presented in Fig. 9. Here we see that the effect of N on $\tilde{q}_{max}$ is almost nonexistent, especially at $Re_L = 10^2$. This conclusion has practical relevance, because it means that there is little benefit in dividing a fixed heat transfer area into smaller plates (i.e. smaller swept lengths b). A weak $\tilde{q}_{max}$ maximum with respect to N develops near $N = 4$ as the Reynolds number increases. The strong effect on $\tilde{q}_{max}$ is due to Re_L, in fact, $\tilde{q}_{max}$ increases almost proportionally with Re_L regardless of the values of N.

The effect of changing the stagger parameter $\tilde{\beta}$ was investigated in two ways. In Fig. 10 the spacing $\tilde{W}$ was set equal to the optimal value $\tilde{W}_{opt}$ that corresponds to perfectly staggered plates ($\tilde{\beta} = 1$). As the stagger parameter varies over the 0–1 interval, the overall thermal conductance exhibits a maximum at a certain $\tilde{\beta}$ value (called $\tilde{\beta}_{opt}$). This maximum becomes sharper as A decreases below $A = 1$: in this range the stagger associated with maximum $\tilde{q}$ is closely approximated by $\tilde{\beta}_{opt} = A$. Perfectly staggered plates ($\tilde{\beta} = 1$) are always better than in-line plates ($\tilde{\beta} = 0$); however, $\tilde{\beta} = 1$ is not the optimal stagger parameter when $A < 1$. Figure 10 also shows that when $A > 1$ the effect of $\tilde{\beta}$ on $\tilde{q}$ is relatively insignificant.

The alternative is to determine the optimal spacing that corresponds to each value of the stagger parameter, namely $\tilde{W}_{opt}(\tilde{\beta})$. This route was followed in the construction of Fig. 11, where $A = 0.5$, $N = 4$ and $Re_L = 10^3$. The optimal spacing increases by roughly 7% as $\tilde{\beta}$ decreases from 1 to 0. In other words, the optimal spacing for in-line plates is slightly larger than for perfectly staggered plates. The corresponding $\tilde{\beta}$ effect on the maximized overall conductance is also

small (within 6%). There is a weak $\tilde{q}$ maximum at $\tilde{\beta} \cong 0.5$, and, as might be expected, we learn again that perfectly staggered plates ($\tilde{\beta} = 1$) perform better than in-line plates ($\tilde{\beta} = 0$).

5. DISCUSSION

In this study we demonstrated experimentally the existence of an optimal spacing for staggered plates in a fixed volume with forced convection. We then simulated the main features of the heat transfer configuration numerically, and investigated systematically the effect of spacing ($\tilde{W}$), channel contact area (A), number of plates in one channel (N), and stagger parameter ($\tilde{\beta}$). The objective of the numerical work was to compare the performance of many geometric arrangements that differ only slightly from one another. For this we had to rely on a numerical approach that was cost-effective, accurate and tested.

For all these reasons, the numerical work was not designed to reproduce in fine detail the geometry that was tested in the laboratory. The experimental configuration (Fig. 2) was limited by the size of the tunnel and the size of the instrumented plates, while in the numerical configuration (Fig. 1) we had to assume a large array (H $\gg$ W) so that we can perform calculations in a single elemental channel. In the experimental set-up, there was also a certain amount of bypass air flow around the array (along the walls of the tunnel). In spite of these differences, a comparison between the experimental results and the 'closest' numerical results available is recommended. Such a comparison is presented in Table 1, which shows that there is reasonable agreement between the two sets of results. The agreement with respect to the optimal spacing is remarkable in view of the differences between the experimental and numerical models. This agreement adds to the earlier conclusion [7–13] that the volume-constrained geometric optimization is 'robust', in the sense that the optimal geometric arrangement is relatively insensitive to finer details of the solid surfaces (shapes, thermal boundary conditions). For example, ref. [7] showed that the optimal spacing is the same for parallel isothermal plates and parallel uniform-flux plates.

Another way to review the present results is to compare them with the correlating theory [7] that was developed for the optimal spacing between continuous parallel plates of length L and plate-to-plate spacing D. The theory is based on intersecting analytically the asymptotes for large spacing and small spacing of the heat transfer rate (Q) of the entire volume. The small-D asymptote showed that Q decreases as D decreases, because in this limit the channels close and the coolant flow ceases. Along the large-D asymptote, Q again decreases as D increases, because the total heat transfer area decreases. These trends guarantee that a maximum Q exists at an intermediate D, which can be estimated by intersecting the two asymptotes. The theoretical spacing (D_{opt}) for maximum Q predicted by the analytical method [7, 11, 26] is

$$\frac{D_{opt}}{L} \cong 2.73\left(\frac{\mu\alpha}{L^2\Delta P}\right)^{1/4}. \tag{11}$$

To convert this estimate to the notation of Fig. 1 we replace L with b, and D_{opt} with W_{opt}. In addition, we note [11] that the scale of the pressure drop across the entire assembly is $(1/2)\rho U_\infty^2$. Equation (11) becomes

$$\tilde{W}_{opt} \cong 3.2Pr^{-1/4}\left(Re_L\frac{N}{A}\right)^{-1/2}. \tag{12}$$

Figure 12 shows that if we replot the data of Fig. 5 in the manner suggested by equation (12) we obtain a very close correlation, in which the theoretical factor 3.2 is replaced by 5.4.

The maximum heat transfer rate that corresponds to the intersection of the small-D and large-D asymptotes of the space with continuous plates of length L is of the order of [7]

$$\frac{Q_{max}}{B} \sim \left(\frac{\rho\Delta P}{Pr}\right)^{1/2} Hc_p(T_w - T_\infty). \tag{13}$$

Recalling that $Q = qH/W$ and $\Delta P \sim (1/2)\rho U_\infty^2$, we can rewrite equation (13) in terms of the dimensionless $\tilde{q}$ defined in equation (3):

$$\tilde{q}_{max} \sim Pr^{1/2}Re_L. \tag{14}$$

Table 1. Comparison of the experimental and numerical results obtained for $A = 1$ and $N = 4$

	Experimental		Numerical	
Re_L	$\tilde{W}_{opt}$	$\tilde{q}_{max}$	$\tilde{W}_{opt}$	$\tilde{q}_{max}$
1000	0.095	484	0.089	319
2000	0.092	595	0.062	646

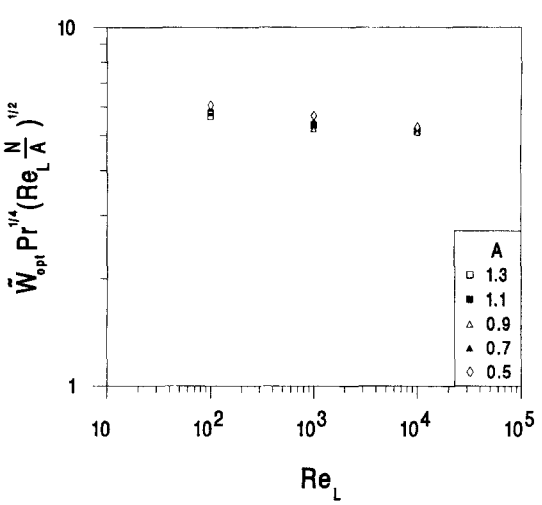

Fig. 12. The correlation of the optimal spacing data shown in Fig. 5.

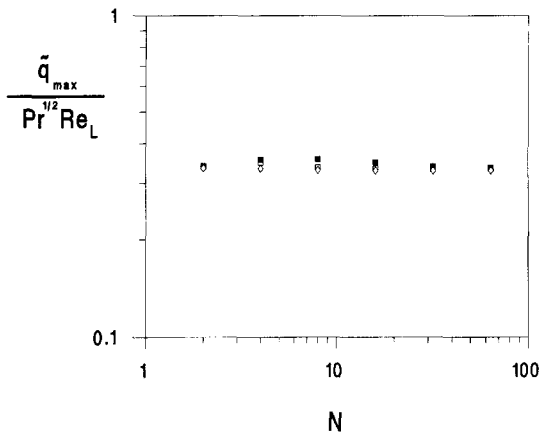

Fig. 13. The correlation of the maximum heat transfer rate data shown in Fig. 9.

Figure 13 shows that this scaling law works very well towards correlating the data reported earlier in Fig. 9. In addition, Fig. 13 shows that the numerical coefficient in the proportionality (14) is a number of order one, which is again in agreement with the theory of refs. [7, 26].

6. CONCLUSION

We have shown experimentally and numerically that the geometric arrangement of staggered plates can be optimized for maximum heat transfer (or maximum thermal conductance) when the optimization is subjected to an overall volume constraint. The staggered-plates arrangement is the latest in a series of basic, even simpler configurations (parallel plates, parallel cylinders) in which the opportunity for volume-constrained heat transfer augmentation has also been demonstrated, for both natural and forced convection [2–13]. Furthermore, the theory of intersecting the two asymptotes (small spacing vs large spacing) [7, 26], which had already been tested in several experiments [6, 8, 10–13], showed once again that it is possible to anticipate the optimal spacing of staggered plates, and the associated thermal conductance maximum.

The present study was formulated as a fundamental volume-constrained geometric optimization problem. The direct application of its results depends on how closely Fig. 1 matches the configuration contemplated in the design of an actual device. There are additional fundamental configurations [6, 7, 11–13] with which the contemplated device could be compared so that its approximate optimal geometry can be predicted. If a more refined optimization is necessary, then this final phase could be pursued in the laboratory, or numerically, by testing only a small number of nearly optimal alternatives. An example of this more comprehensive and interactive work is provided by ref. [27]. The important contribution of the present paper (in fact, the contribution of fundamental work in general) is 'to show the way' for the more applied work that will follow: specifically, we know now that geometric optima exist, and that they can be predicted at least approximately.

REFERENCES

1. Peterson, G. P. and Ortega, A., Thermal control of electronic equipment and devices. *Advances Heat Transfer*, 1990, **20**, 181–314.
2. Bar-Cohen, A. and Rohsenow, W. M., Thermally optimum spacing of vertical, natural convection cooled, parallel plates. *Journal of Heat Transfer*, 1984, **106**, 116–123.
3. Bejan, A., *Convection Heat Transfer*. Wiley, New York, 1984, p. 157, problem 11.
4. Kim, S. H., Anand, N. K. and Fletcher, L. S., Free convection between series of vertical parallel plates with embedded line heat sources. *Journal of Heat Transfer*, 1991, **113**, 108–115.
5. Anand, N. K., Kim, S. H. and Fletcher, L. S., The effect of plate spacing on free convection between heated parallel plates. *Journal of Heat Transfer*, 1992, **114**, 515–518.
6. Bejan, A., Fowler, A. J. and Stanescu, G., The optimal spacing between horizontal cylinders in a fixed volume cooled by natural convection. *International Journal of Heat and Mass Transfer*, 1995, **38**, 2047–2055.
7. Bejan, A. and Sciubba, E., The optimal spacing of parallel plates cooled by forced convection. *International Journal of Heat and Mass Transfer*, 1992, **35**, 3259–3264.
8. Mereu, S., Sciubba, E. and Bejan, A., The optimal cooling of a stack of heat generating boards with fixed pressure drop, flowrate or pumping power. *International Journal of Heat and Mass Transfer*, 1993, **36**, 3677–3686.
9. Bejan, A. and Morega, A. M., The optimal spacing of a stack of plates cooled by turbulent forced convection. *International Journal of Heat and Mass Transfer*, 1994, **37**, 1045–1048.
10. Morega, A. M., Bejan, A. and Lee, S. W., Free stream cooling of a stack of parallel plates. *International Journal of Heat and Mass Transfer*, 1995, **38**, 519–531.
11. Morega, A. M. and Bejan, A., Optimal spacing of parallel boards with discrete heat sources cooled by laminar forced convection. *Numerical Heat Transfer, A*, 1994, **25**, 373–392.
12. Stanescu, G., Fowler, A. J. and Bejan, A., The optimal spacing of cylinders in free-stream cross-flow forced convection. *International Journal of Heat and Mass Transfer*, 1996, **39**, 311–317.
13. Bejan, A., The optimal spacing for cylinders in crossflow forced convection. *Journal of Heat Transfer*, 1995, **117**, 767–770.
14. Kays, W. M. and London, A. L., *Compact Heat Exchangers*, 3rd edn. McGraw-Hill, New York, 1984.
15. Kakac, S., Bergles, A. E. and Mayinger, F. eds, *Heat Exchangers: Thermal–Hydraulic Fundamentals and Design*. Hemisphere, Washington, DC, 1981.
16. Shah, R. K. and Mueller, A. C., Heat exchangers. In *Handbook of Heat Transfer Applications*, 2nd edn, Chap. 45, ed. W. M. Rohsenow, J. P. Hartnell and E. N. Ganic. McGraw-Hill, New York, 1985.
17. Guglielmini, G., Nannei, E. and Tanda, G., Natural convection and radiation heat transfer from staggered vertical fins. *International Journal of Heat and Mass Transfer*, 1987, **30**, 1941–1948.
18. Tanda, G., Natural convection heat transfer from a staggered vertical plate array. *Journal of Heat Transfer*, 1993, **115**, 938–945.
19. Moffat, R. J., Describing uncertainties in experimental

results. *Experimental Thermal Fluid Science*, 1988, **1**, 3–17.
20. Kline, S. J. and McClintock, F. A., Describing uncertainties in single-sample experiments. *Mechanical Engineering*, 1953, **75**, 3–8.
21. Howle, L., Georgiadis, J. and Behringer, R., Shadowgraphic visualization of natural convection in rectangular-grid porous layers. *ASME HTD*, 1992, **206–1**, 17–24.
22. Dally, J. W., Riley, W. F. and McConnell, K. G., *Instrumentation for Engineering Measurements*. Wiley, New York, 1993, p. 425.
23. Mochizuki, S. and Yagi, Y., Characteristics of vortex shedding in plate array. In *Flow Visualization II*, ed. W. Merzkirch. Hemisphere, Washington, DC, 1980, pp. 99–103.
24. Fowler, A. J. and Bejan, A., Forced convection in banks of inclined cylinders at low Reynolds numbers. *International Journal of Heat & Fluid Flow*, 1994, **15**, 90–99.
25. *FIDAP Theory Manual*. Fluid Dynamics International, Evanston, IL, Vol. 7.0 (1993).
26. Bejan, A., *Heat Transfer*. Wiley, New York, 1993, pp. 331–332.
27. Zhu, N. and Vafai, K., Optimization analysis of a disk-shaped heat pipe. *Journal of Thermophysics and Heat Transfer*, 1996, **10**, 179–182.